

Fabian Guse^{1,*}
Maximilian Voshage²
Johannes H. Schleifenbaum²
Katharina Schmitz¹


Cavitation Erosion Resistance of Additively Manufactured Materials

Cavitation-induced wear, also known as cavitation erosion, can be found in many fluid power components, especially in water hydraulics. Cavitation erosion leads to component damage and might even cause system failure. The resistance of various materials to cavitation erosion when using conventional manufacturing processes has already been investigated in the past. In this work, the effects of additively manufactured materials on the resistance to cavitation erosion are investigated and compared to effects after conventional manufacturing. Also, the influence of the build-up direction of the additively manufactured specimens on cavitation erosion is determined. As the main indicators of cavitation erosion, mass loss and the surface structure are determined for all specimens.

Keywords: Additive manufacturing, Cavitation erosion, Experimental investigation, Wear

Received: August 20, 2022; *revised:* September 01, 2022; *accepted:* September 09, 2022

DOI: 10.1002/ceat.202200340

 This is an open access article under the terms of the Creative Commons Attribution-NonCommercial-NoDerivs License, which permits use and distribution in any medium, provided the original work is properly cited, the use is non-commercial and no modifications or adaptations are made.

1 Introduction

The durability of hydraulic components is often limited by wear. In addition to mechanical wear, cavitation-induced wear, which is also known as cavitation erosion, can be found in fluid power components, especially in water hydraulics. Three different types of cavitation can be distinguished: vapor cavitation, gas cavitation, and pseudo-cavitation [1]. Vapor cavitation is a phenomenon that occurs in fluids when the static pressure is reduced below the vapor pressure, which can happen in critical flow conditions and adverse operating points. Consequently, bubbles are formed and transported to regions of higher pressures, where they collapse, releasing a significant amount of kinetic energy. Vapor cavitation represents the most energetic and destructive form of cavitation [2]. As a consequence, this work focuses on the aforementioned vapor cavitation and its effects.

As the surrounding pressure rises again, the bubbles implode spherically in the liquid and cause a shock wave. If the bubbles are in close proximity to or in direct contact with a material surface, an asymmetric collapse can be observed. This generates a high-energy liquid jet (microjet) directed at the surface, which can reach a velocity of up to 410 m s^{-1} , high temperature, and high pressure [3]. If this collapse occurs in the vicinity of the component's walls, material damage can be observed. This phenomenon is called cavitation erosion, which can lead to component failure [1]. So far, there is no material known to be resistant to cavitation erosion.

The resistance of different materials to cavitation erosion when using conventional manufacturing processes has already been investigated in the past. Extensive studies have been performed by Berger [4], who investigated the mass loss of the most common conventionally manufactured metals. Utilizing the concept of flow cavitation, the mass loss of steel, cast iron,

and several alloys was determined. An empirical equation was formulated, which allows determining the mass loss as a function of Young's modulus, the yield strength, the ultimate tensile strength, and the hardness. The hardness was determined to have the biggest impact: doubling the hardness leads to an approximate quartering of the mass loss rate.

For a good comparability of the results, a controlled cavitation environment must be generated. In the literature, a distinction is made between oscillatory cavitation and flow cavitation. Both methods reproducibly reduce the static pressure below the vapor pressure of the fluid. In oscillatory cavitation, the pressure drop is generated by a vibrating apparatus that "ruptures" the fluid and causes cavitation bubbles to form [2]. With an ultrasonic sonotrode submerged in a fluid, the fluid can be excited so that the local pressure decreases and cavitation bubbles form. In hydraulics, however, flow cavitation occurs much more frequently. In contrast to oscillation cavitation, flow cavitation is found in hydraulic components, e.g. in valves, when a high pressure drop due to constrictions leads to an acceleration of the fluid. As a consequence, an increase in velocity results in a further reduction of the static pressure, leading to cavitation. In order to reproduce flow cavitation in a corresponding test setup, fluid is expanded in a nozzle or an orifice. Due to the large pressure difference, a high-velocity fluid free jet develops, which is aimed directly at a sample

¹Fabian Guse, Prof. Dr.-Ing. Katharina Schmitz
fabian.guse@rwth-aachen.de, fabian.guse@ifas.rwth-aachen.de
RWTH Aachen University, Institute for Fluid Power Drives and Systems (ifas), Campus-Boulevard 30, 52074 Aachen, Germany.

²Maximilian Voshage, Prof. Dr.-Ing. Johannes H. Schleifenbaum
RWTH Aachen University, Digital Additive Production (dap), Campus-Boulevard 73, 52074 Aachen, Germany.

surface. The free jet and sample are submerged into the fluid so that a cloud of cavitation bubbles forms in the direction of the sample surface, where cavitation erosion occurs. In order to compare different flow conditions, the cavitation number σ is introduced, which is a dimensionless number describing the pressure reduction in the orifice.

$$\sigma = \frac{p_d - p_v}{\frac{1}{2}\rho v^2} \quad (1)$$

In Eq. (1), p_d is the local downstream pressure after the orifice, p_v is the vapor pressure, ρ is the density of the liquid, and v is the velocity of the fluid free jet.¹⁾ The dynamic pressure (term in the denominator) can be determined when the upstream and downstream pressures are known. The cavitation number is one of the very few means to characterize a cavitating flow and has been thoroughly investigated by Gevari et al. [5].

For some time now, additive manufacturing, in particular laser powder bed fusion (LPBF), has been gaining increasing importance in fluid power technology. This manufacturing technology enables novel, improved designs and allows for the optimization of hydraulic components with respect to pressure losses, component mass, or volume. The process of LPBF works as follows: For the data preparation, a computer-aided design (CAD) model of the component needs to be sliced in layers with a defined thickness. In the LPBF process, metal powder is distributed uniformly by a powder recoater, to the set layer thickness, on a vertically movable build platform. For each layer, the area to be solidified is scanned by a laser via deflection mirrors and a set of parameters. The build plate is subsequently lowered by one layer and new powder is distributed.

This cycle is repeated until the component is completely built up, layer by layer. However, the manufacturing process induces a high surface roughness and an anisotropy, which is inherent to the layer-by-layer manufacturing and often requires post-processing such as heat treatment. Although grinding or polishing allows an increase of the surface quality, in many cases (e.g. in flow channels), a proper post-processing is not possible or economically reasonable.

Although LPBF is a very promising method for the future design process of hydraulic components, there are several risks and unknown factors that need to be investigated and accounted for. For instance, the effect of LPBF on the resistance to cavitation erosion has not yet been sufficiently investigated, especially when including the effect and the influence of the build-up direction. Studies conducted by Ding et al. [6] and Zou et al. [7] show that the cavitation erosion resistance of additively manufactured samples differs from those manufactured conventionally, resulting in different mass loss rates at different times. They investigated the influence of the material microstructure on its cavitation erosion resistance. The grain level microstructure is directly affected by the process parameters during LPBF (e.g., the laser scanning speed and the laser power). Harges et al. [8] furthermore focused on the micro-

structural grain defects, which are inherent to the LPBF process, but they did not observe a significant difference in cavitation erosion resistance between conventionally and additively manufactured samples of the same material. Two additively manufactured aluminum alloys were compared in the study of Tocci et al. [9]. They concluded that the alloying components also have an effect on the cavitation erosion resistance. In contrast to the current study, all results mentioned above, except for those obtained by Zou et al. [7], were attained using an ultrasonic vibratory cavitating system in accordance with the ASTM standard G32-16. Consequently, their methods do not represent the actual type of cavitation damage found in additively manufactured hydraulic parts [10]. Furthermore, all of them used a reworked specimen surface and some applied thermal post-processing.

In this work, LPBF samples made of stainless steel (1.4404) and aluminum (AlSi10Mg) were compared with conventionally manufactured samples made of the same materials. Special attention was paid to maintain the “as-built” surface as no post-processing was performed. In addition to the usual direction of build-up, i.e. parallel to the building plate, different angles of 45° and 90° to the building plate were also examined for the additively manufactured aluminum specimens. In order to assess the resistance to cavitation erosion, all test specimens were tested on a cavitation test rig, where they were exposed to a cavitating flow, as opposed to ultrasonic cavitation. This cavitation jet was produced employing an orifice flow, and a water-based HEA fluid was used. Due to the impinging cavitating flow, a mass loss could be observed, which was determined for all specimens. In addition, the change of the surface structure over time was observed using the optical method of focus variation. The results are supported by roughness and hardness values.

2 Experimental Setup

The objective of the experimental investigation is to characterize the cavitation erosion resistance of various materials and manufacturing methods. First, the reproducible generation of the cavitation environment is described. This is followed by the classification of the samples into categories and a description of their properties. Finally, the measurement method is described.

2.1 Test Setup

The LPBF experiments were performed on an EOS M290 system designed by Electro Optical Systems (EOS GmbH, Kallungen, Germany); the system has been specifically developed for manufacturing on the industrial scale. The beam source is a single-mode fiber laser (wavelength of 1064 nm) with up to 400 W of power output. Samples were manufactured on steel or aluminum baseplates, using a bidirectional scanning strategy with 67° rotation between consecutive layers.

For the presented experimental investigation, the method of “cavitating jets” was used. The cavitation jet is generated in accordance with the ASTM standard G134-17. Cavitation

1) List of symbols at the end of the paper.

bubbles are generated by expanding a liquid utilizing an orifice flow, subsequently hitting the sample surface [11]. According to Lichtarowicz [12], this test setup is characterized by high reproducibility. The experimental conditions can be easily adjusted and remain largely constant over the duration of the experiment [12]. This form of cavitation is more suitable for recreating conditions that can be found in hydraulic applications like valve flows.

The circuit diagram in Fig. 1 shows the test rig setup. It is operated with a water-based HFA fluid containing 97 % water. Because of its high water content, the vapor pressure ($p_v = 100$ mbar at 50°C) is higher than those of other fluids based on mineral oil, leading to a more pronounced effect of cavitation.

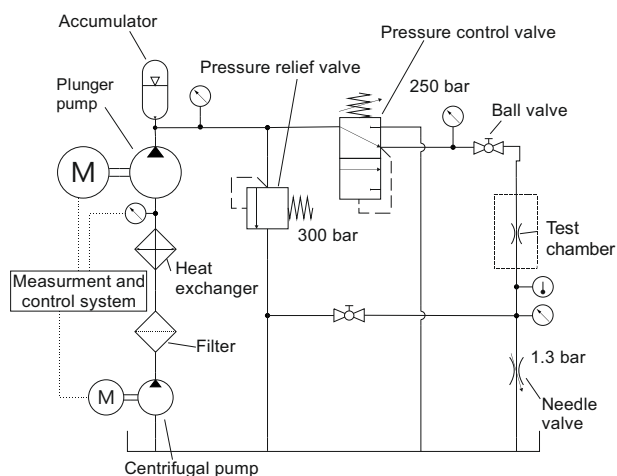


Figure 1. Circuit diagram of the test setup.

Starting with the tank, a centrifugal pump conveys the fluid through a filter and to a heat exchanger. Due to heat generation by fluid friction, an equilibrium temperature between 32 and 37°C is maintained. As shown by Dular [13], the temperature is an important factor influencing the cavitation tendency, as the vapor pressure of water is highly dependent on the temperature. It is therefore necessary to guarantee constant conditions at all times. The fluid is pumped by the subsequent plunger pump. In order to avoid cavitation at the plunger pump suction side, the upstream centrifugal pump is used to increase the pressure level, and a flexible hose dampens pressure fluctuations. An accumulator is implemented between the plunger pump and the test chamber to dampen out pressure ripples due to volume flow pulsation of the plunger pump.

A downstream pressure control valve regulates the test chamber inlet pressure to 250 bar. The backpressure behind the nozzle (i.e., within the test block) is set to 1.3 bar via a needle valve. At this pressure, a uniform bubble jet is formed. For this investigation, the optimum backpressure derived by Kleinbreuer [2] was utilized, who investigated the correlation between backpressure and cavitation erosion. A temperature sensor in the return line records the fluid temperature.

Fig. 2 shows a sectional view of the test chamber, in which the actual process of cavitation erosion takes place. The setup is based on the investigations by Kleinbreuer [2] and Berger [4]. A sealed chamber cover is screwed to the housing. The

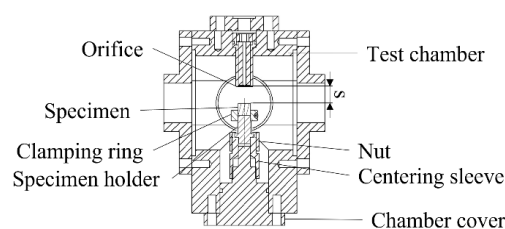


Figure 2. Sectional view of the test chamber.

centering sleeve sits concentric to the chamber cover and is fastened with a thread. The thread allows adjustment of the distance s between the specimen surface and the orifice. A nut fixes the specimen holder to the centering sleeve. The specimen is fitted to the specimen holder on the lateral surface by a clamping ring, so that the face of the specimen points in the direction of the orifice.

Due to the pressure difference, the fluid enters the chamber via an orifice at high velocity. The chamber is completely filled with fluid. The orifice bore has a diameter of $450\ \mu\text{m}$. Due to the expansion of the fluid, a free cavitation jet is formed, which can be characterized by a cavitation number according to Eq. (1) of $s = 4.83 \times 10^{-3}$. The free jet exits the orifice and impinges on the face of the cylindrical specimen, subsequently leading to cavitation erosion. For the purpose of repeatable and precise positioning of the specimen after removal and reclamping, an optical mark is added to the specimen and the specimen holder.

The orifice is located at a distance $s = 21$ mm from the surface of the specimen. This distance provides the optimal lifetime for the cavitation bubbles to implode energetically on the specimen surface [2]. Furthermore, a preliminary investigation showed that mass removal is maximized at this distance.

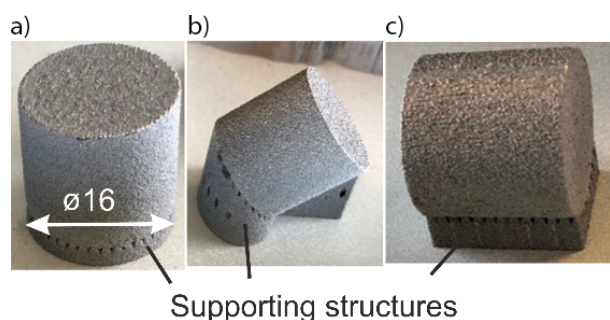
2.2 Material and Test Specimens

The specimens in this investigation were manufactured additively as well as conventionally. The materials used were stainless austenitic steel 1.4404 (AISI: 316L) and the aluminum alloy AlSi10Mg. All specimens have a cylindrical shape with a height of 15 mm and a diameter of 16 mm.

The specimens are divided into six groups depending on their configuration. Two groups are made out of stainless steel and four out of aluminum. Each group consists of five specimens in order to ensure reproducibility. One group per material serves as a control group and was produced in a conventional casting process with subsequent machining. The additively manufactured specimens of both materials were produced using the EOS M 290 manufacturing system, with the process parameters listed in Tab. 1. For the additively manufactured aluminum specimens, the build orientation was varied. One group was built up layer by layer parallel to the base plate (0°), and one with the central axis inclined by 45° , as can be seen in Fig. 3. The specimens of the third group were fabricated with a 90° rotated central axis. The necessary support structures were removed afterwards. No thermal post-processing was applied, and the front face, which was exposed to the free cavitation jet, was not reworked after the manufacturing process. This allows

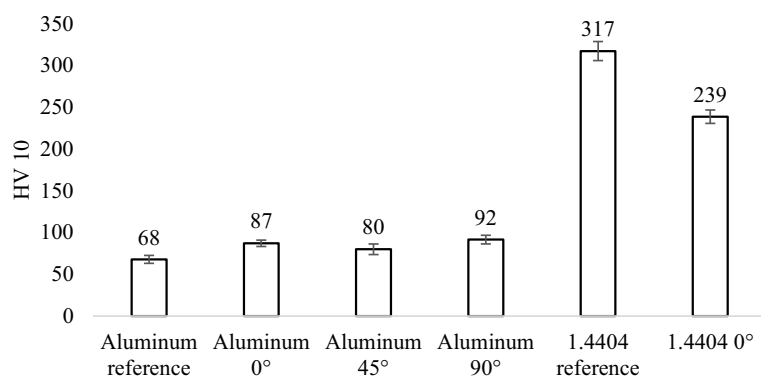
Table 1. Process parameters for additive manufacturing of stainless-steel and aluminum specimens.

	Aluminum AlSi10Mg	Stainless steel 1.4404
Particle size	10–45 μm	10–45 μm
Laser power	200 W	105 W
Focus diameter	74 μm	74 μm
Scanning speed	1400 mm s^{-1}	800 mm s^{-1}
Hatch distance	100 μm	70 μm
Layer thickness	30 μm	30 μm
Volume energy density	47.6 W mm^{-3}	62.5 W mm^{-3}

**Figure 3.** Additively manufactured aluminum specimens in different orientations including support structures: (a) at 0°, (b) at 45°, (c) at 90°.

a direct comparison of the as-built surfaces and their cavitation erosion behavior according to the direction of build-up.

Since the hardness of a material is decisive for its cavitation erosion resistance as described in the introduction, the hardness of all specimens was determined employing a Vickers hardness (HV) test. The results are shown in Fig. 4. The conventionally manufactured stainless-steel specimens (1.4404 reference) with a hardness of 317 HV 10, followed by the additively manufactured counterpart (1.4404 0°) with 239 HV 10, are the hardest specimens in this investigation. The conventionally manufactured aluminum samples (aluminum reference) exhibit the lowest hardness at 68 HV 10. The additively

**Figure 4.** Initial hardness of the specimens.

manufactured aluminum specimens are slightly harder than the conventionally manufactured aluminum specimens. In addition, the measured hardness differs slightly depending on the build-up direction, although – with regard to the standard deviation – the difference is negligible and an influence of the build-up direction regarding the hardness of the samples cannot be concluded.

3 Results

The evaluation of the tests initially focuses on the mass loss of the specimens over the test period, as the mass loss is the principal measure for determining the cavitation erosion resistance of a material. Subsequently, the results of the roughness measurement and optical surface examination are presented. The change of the surface quality is examined as well, providing information about the underlying mechanisms.

3.1 Mass Loss

The mass loss of a sample was calculated before and after exposing it to the cavitation environment. Between two measurements, the specimen was exposed for 2 h. A precision laboratory balance with an accuracy of 10 μg was used to measure the mass. For each group consisting of five specimens, an averaged difference value was calculated. Figs. 5 and 6 show the cumulative mass removal of all aluminum and stainless-steel groups. In the case of aluminum, the configuration that was additively manufactured at an angle of 90° shows the highest mass removal of 17.79 mg after 8 h of testing. The aluminum specimens additively manufactured at an angle of 45° show an average cumulative mass removal of 13.044 mg. The conventionally fabricated reference aluminum specimens have a mass removal of 11.356 mg, which is more than twice as large as for the additively fabricated specimens that were built up parallel to the build plate. At 4.450 mg, these show the lowest mass removal for aluminum and a remarkably low variation between the samples.

In direct comparison to aluminum, the additively manufactured stainless-steel specimens show a much lower mass loss. This was expected due to the increased hardness of steel. With a mass loss of 1.414 mg, the additively manufactured stainless-steel specimens (1.4404 0°) show a mass removal lower than one-third compared to aluminum. The reference steel sample shows a mass loss of 0.309 mg, thus being the most cavitation-resistant group.

For all additively manufactured specimens, it is noticeable that the average mass removal rate is higher in the first two hours than in the following hours. For most specimens, approximately 50 % of the total mass removal is realized in these first two hours. The remaining mass removal is evenly distributed over the rest of the test period. The average mass removal rate during this period (2–8 h) is almost identical for aluminum 45° with 1.125 mg h^{-1} and aluminum 90° with 1.214 mg h^{-1} ,

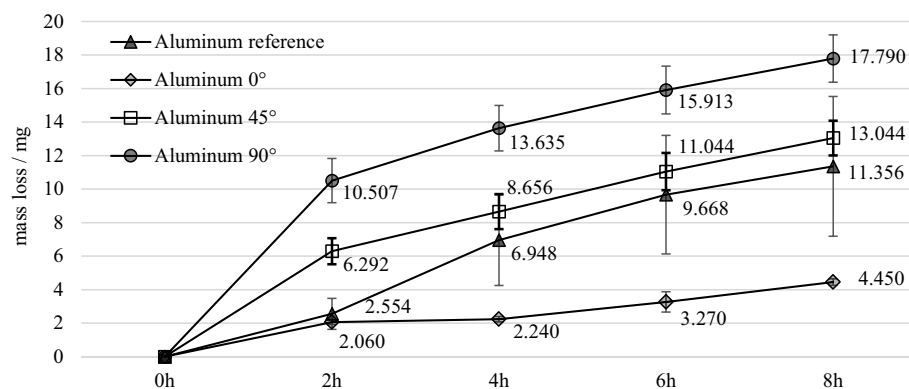


Figure 5. Cumulative mass removal of aluminum.

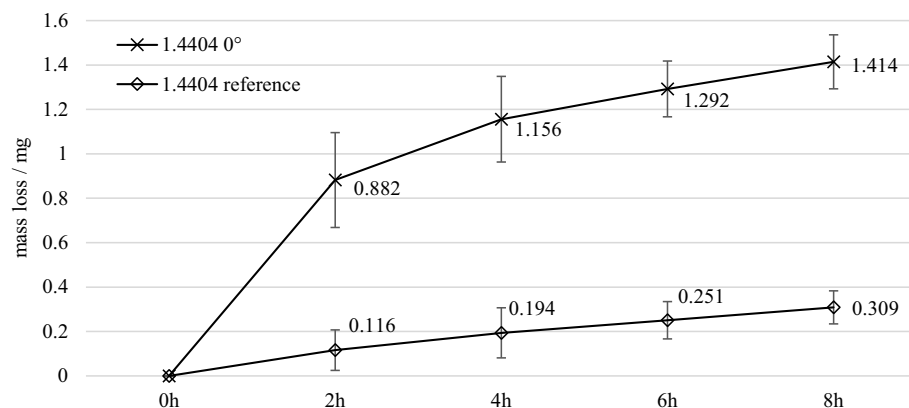


Figure 6. Cumulative mass removal of stainless steel.

whereas 1.4404 0° with 0.089 mg h^{-1} shows the lowest mass removal rate of the additively manufactured samples. The implications of these findings will be elaborated in Sect. 4.

Unlike the groups of additively manufactured samples, the group of conventionally manufactured samples (aluminum and stainless steel) shows an almost equal mass removal rate in the first two hours compared to the rest of the test run. On average, the mass removal rate is 1.42 mg h^{-1} for the conventional aluminum samples. The conventionally manufactured stainless-steel specimens show an average mass removal rate of 0.039 mg h^{-1} over the entire test period. Due to the comparatively low mass removal rate, the effect of the build-up direction for the additively manufactured stainless steel was not investigated any further.

3.2 Surface Quality

In addition to the mass loss and hardness, the shape and roughness of the specimen surfaces were determined, using the focus variation microscope InfiniteFocus from Bruker Alicona. Using the principle of focus variation, a 3D scan of the surface was created. The change in surface texture and thus the development of damage due to cavitation erosion can be investigated. Similar to the mass loss investigations, each sample was exposed to the jet cavitation environment for a period of 8 h,

interrupting the experiment every 2 h and performing a surface measurement.

The resulting 3D image was analyzed by evaluating a profile path on the sample surface along its complete diameter. In this investigation, an averaged profile path was utilized and created from 300 individual parallel measurement paths. Each measurement path captures the height profile of the surface over its length. The averaging of several measurement profiles serves to reduce the need for exact repositioning under the microscope. The rotational position of the specimen is reproduced in between two measurements. The starting coordinates and the path length are maintained for each sample, as well.

In Fig. 7, the profile paths of the aluminum specimens before conducting the experiment are shown, as well as those after 2, 4, 6, and 8 h. At every measurement time, an averaged profile path was created for each group consisting of five specimens.

As can be seen, at the center of each sample a funnel-shaped indentation forms over time. The

depth of this indentation increases uniformly during the course of the test. After 8 h, the largest difference to the initial state is found in the center of the reference aluminum samples. The smallest change can be seen in the additively manufactured samples with a manufacturing angle of 0°. Adjacent to the center, the aluminum specimens show a circular zone with no or very little damage. Almost no change in the profile depth can be seen in this area. In the case of aluminum 45°, this zone is less pronounced. This zone is followed by another circular zone characterized by increased material erosion. Radial symmetrical valleys can be observed, which are overlapped by individual smaller indentations. This zone is particularly deep and distinct for the conventionally manufactured aluminum samples. Adjacent to the damaged circular ring zone, an undamaged zone is visible that does not change significantly over the course of the experiments.

4 Discussion

The primary indicator for determining a material's resistance against cavitation erosion is the mass loss. This measure is transferred into a mass erosion rate over the test period. In principle, the lower the mass erosion rate, the higher is the cavitation erosion resistance of a material group. Surface roughness and hardness serve as the basis for an explanation.

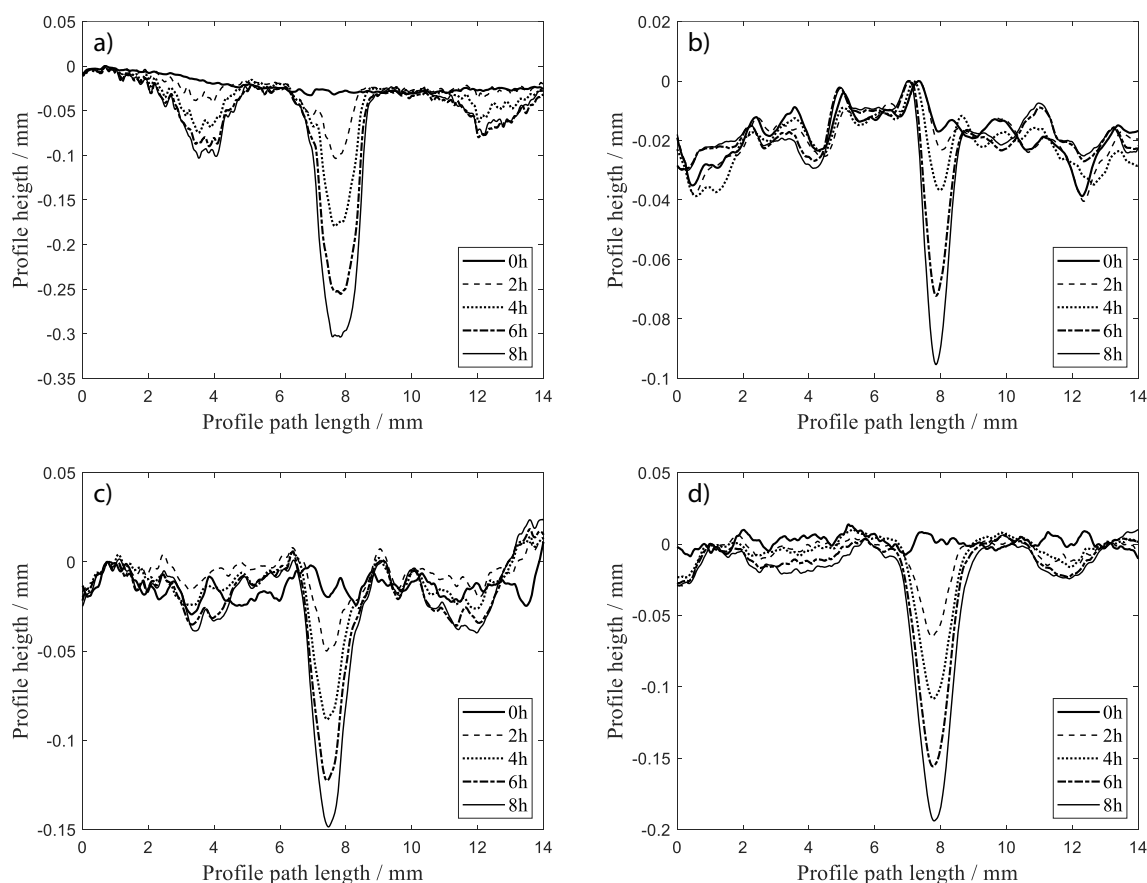


Figure 7. Changing surface quality of the aluminum alloys: (a) aluminum reference, (b) aluminum 0°, (c) aluminum 45°, (d) aluminum 90°.

The differences in cavitation erosion resistance between the two materials, aluminum (AlSi10Mg) and stainless steel (1.4404), were presented in Figs. 5 and 6. The mass loss for the conventionally manufactured aluminum samples is 40 times higher than the mass loss for the conventionally manufactured stainless-steel samples. The significantly higher resistance of the stainless-steel specimen is due to its higher hardness, which has been investigated by Kleinbreuer [2] and Berger [4]. The relationship between the hardness and the cavitation erosion resistance is already known in the literature and is here consistent with the results obtained in the cited publications.

However, as can be seen in Figs. 4 and 5, although the hardness of the additively manufactured aluminum specimens is almost independent of the build direction, the absolute mass removal *does* vary depending on this parameter. It can therefore be concluded that the surface roughness, which is considerably larger for the additively manufactured specimens, is a factor that has to be considered for explaining the material loss. More precisely, a rougher specimen surface leads to an increased mass removal. Kleinbreuer [2] came to similar conclusions in his study. He considered finely machined surface structures and explained the increased mass removal with the lower mechanical strength of the roughness peaks, which were first damaged and then removed as a result of the high-energy implosion inherent to cavitation. In the present work, the

surfaces of the specimens were not reworked. The fissured and rough surface structures of the additively manufactured aluminum specimens, as depicted in Fig. 7, suggest that the roughness peaks are primarily damaged here, as well.

In the first two hours of the experiment, a noteworthy feature can be seen in all additively manufactured specimens. For both materials, the mass removal rate is higher than in the following six hours, as can be seen in Figs. 5 and 6. This behavior cannot be observed for the reference samples. These observations match those made by Ding et al. [6] and Zou et al. [7] and could be explained with the existence of sintered powder particles on the LPBF “as-built” surface. Since the front surfaces of the additively manufactured samples at 45° and 90° consist not only of one but of many individual melting layers, they are open-pored. The specimens manufactured with an angle of 0° do not show the surface structure but have a much more homogeneous surface. Consequently, for an inclined manufacturing angle, the probability of metal powder adhering to the surface is higher. These particles offer little resistance to cavitation erosion and are removed first. These results are consistent to those of Zou et al. [7] and Hardes et al. [8]. Furthermore, the comparison of the stainless-steel specimens shows that the additively manufactured specimens have a higher mass removal rate than the conventionally manufactured specimens, even after the initial detachment of weakly bonded metal powder.

This is due to both the higher hardness of the conventionally manufactured specimens and the significantly higher surface roughness of the additively manufactured specimens (as can be seen in Figs. 4 and 7).

Additionally, the effects on the component surface should be discussed. As was shown in Fig. 7, two distinct zones develop, which are affected by the cavitating environment. The first zone is the funnel-shaped area in the center of the specimen, where the cavitating jet impinges. This is where the stagnation point of the cavitation free jet is located and where, statistically, most of the bubbles reach the surface and cause material removal. Nevertheless, these indentations could be explained by the high impulse directed onto the surface of the specimens and by small particles, which lead to an abrasive effect. According to Kleinbreuer, however, these latter two explanations can be ruled out: When cavitation is suppressed by slightly increasing the counterpressure in the test chamber while maintaining the same pressure difference across the orifice (i.e., not changing the jet speed or impulse), no damage to the center was visible [2]. Therefore, a cavitation-induced destruction is the most likely explanation. The depth of this indentation steadily increases with the time during which the specimen is exposed to cavitation. The second area is the circular zone characterized by increased material erosion, with a radius of approximately 4 mm. Interestingly, the depth of this second radial zone does not increase steadily but converges after several hours, as can be observed in Fig. 7. This suggests that, above a certain roughness, a constant or decreasing mass removal rate occurs. Kleinbreuer [2] called this phenomenon “hole damping”. Cavitation bubbles settle in deep craters of the fissured surface and form a “protective cushion” [2]. The characteristic profile path in Fig. 7 is due to local flow conditions on the surface. On the one hand, a counterflow to the impinging cavitation jet arises from the central depression due to its geometry. On the other hand, a radial symmetric jet deflection takes place at the stagnation point of the impinging cavitation jet. These two aspects combined contribute to the fact that, in the circular zone adjacent to the center, cavitation blasts do not reach close enough to the surface to cause material removal. Only at a certain distance from the center, cavitation bubbles approach the surface of the material again. This form of damage is also to be expected for the additively manufactured samples. Here, however, the high surface roughness has a greater influence on the path of the cavitation bubbles than the flow effect on the surface. The bubbles are increasingly stopped by the pre-existing roughness peaks and thus are not guided away from the surface by flow effects. The damage is therefore not limited to the circular ring zone, as observed for the conventionally manufactured surfaces. This further complicates the prediction of the exact position of the damage on rough additively manufactured surfaces.

5 Conclusion

Additive manufacturing is becoming increasingly important in hydraulics, and so is the influence of cavitation with respect to additively manufactured materials. In this work, the cavitation erosion resistance of additively manufactured materials using

LPBF and conventionally manufactured specimens was investigated. For this purpose, specimens made of aluminum (AlSi10Mg) and stainless steel (1.4404) were exposed to jet cavitation for a total of 8 h. Regarding the manufacturing of the specimens, the orientation of the specimen surface was varied relative to the build-up direction. Surface orientations parallel to the base plate (0°) and at an angle of 45° and 90° to the base plate were distinguished.

The cavitation free jet was generated utilizing a test setup, by fluid expansion in an orifice with a diameter of 0.45 mm and a pressure in front of the orifice of 250 bar and of 1.3 bar after the orifice. A mixture of water and 3 % HFA liquid was used as the pressure medium. Preliminary investigations were conducted to determine the ideal distance between the orifice and the sample surface. The hardness of the samples was determined and the changes with respect to mass loss and surface topology were considered during the experiments.

The results of this work can be summarized as follows:

- The results suggest that the mass loss due to cavitation erosion of additively manufactured materials is dependent on the direction of the build-up. With an increasing angle between the specimen surface and the base plate during the build-up process, the mass loss due to cavitation erosion increases, as well. More precisely, for the present investigation, aluminum specimens with a build angle of 90° show a higher mass loss than the aluminum specimens built at 45° and 0°. The additively manufactured specimens with a 0° build-up direction showed the lowest mass loss, even compared to the conventionally manufactured samples.
 - Additively manufactured aluminum and stainless-steel specimens show the highest mass removal rate in the first two hours in the cavitation environment. The high surface roughness of the samples results in a shortened incubation phase. After this initial mass loss, the mass removal rate decreases and approaches the mass loss rate of the conventionally manufactured samples. This effect could be explained with the existence of sintered powder particles on the LPBF “as-built” surface, which are being removed due to the influence of the cavitation.
 - The conventionally fabricated stainless-steel specimens show higher resistance to cavitation erosion than the specimens additively fabricated under the 0° build-up direction. Stainless steel also proves to be significantly more resistant than aluminum. Both observations can be explained with an increased hardness.
 - A high surface roughness resulting from the additive manufacturing process also results in a different damage pattern compared to less rough surfaces. The damage pattern is broader and more randomly scattered. This is due to the influence of the roughness peaks, to which bubbles increasingly adhere. This also leads to a less defined erosion pattern compared to the conventionally manufactured material samples.
- Looking ahead, there are some aspects that could be addressed in the future. In this work, the test duration was limited to 8 h. In a further study with a longer test period, it could be investigated how the above-mentioned parameters change in the further course. In addition, the influences of the process parameters of additive manufacturing on the cavitation erosion resistance were not taken into account, which could therefore

be included in further studies. The results obtained in this work could also be supplemented in subsequent work with tests on other materials.

Data Availability Statement

The data that support the findings of this study are available from the corresponding author upon reasonable request.

Acknowledgment

Open access funding enabled and organized by Projekt DEAL. [Correction added on October 20, 2022, after first online publication: Projekt Deal funding statement has been added.]

The authors have declared no conflict of interest.

Symbols used

p_d	[bar]	downstream pressure after the orifice
p_v	[bar]	vapor pressure
s	[m]	distance between orifice and specimen surface
v	[m s ⁻¹]	velocity

Greek symbols

ρ	[kg m ⁻³]	density
σ	[-]	cavitation number

Abbreviations

CAD	computer aided design
HV	Vickers hardness
LPBF	laser powder bed fusion

References

- [1] K. Schmitz, H. Murrenhoff, *Umdruck zur Vorlesung Grundlagen der Fluidtechnik: Teil 1: Hydraulik*, 2nd ed., Reihe Fluidtechnik U, Shaker, Aachen **2018**.
- [2] W. Kleinbreuer, Untersuchung der Werkstoffzerstörung durch Kavitation in ölhydraulischen Systemen, *Ph.D. Thesis*, Rheinisch-Westfälische Technische Hochschule Aachen, Aachen **1979**.
- [3] J. F. Gülich, *Kreiselpumpen*, 4th ed., Springer Vieweg, Berlin, Heidelberg **2004**, pp. 246–323.
- [4] J. Berger, Kavitationserosion und Maßnahmen zu ihrer Vermeidung in Hydraulikanlagen für HFA-Flüssigkeiten, *Ph.D. Thesis*, Rheinisch-Westfälische Technische Hochschule Aachen, Aachen **1983**.
- [5] M. T. Gevari, M. Ghorbani, A. J. Svagan, *AIP Adv.* **2019**, 9, 105012. DOI: <https://doi.org/10.1063/1.5115336>
- [6] H. Ding, Q. Tang, Y. Zhu, et al., *Friction* **2021**, 9, 1580–1598. DOI: <https://doi.org/10.1007/s40544-020-0443-7>
- [7] J. Zou, Y. Zhu, M. Pan, et al., *Wear* **2017**, 376/377, 496–506. DOI: <https://doi.org/10.1016/j.wear.2016.11.031>
- [8] C. Harges, F. Pöhl, A. Röttger, et al., *Addit. Manuf.* **2019**, 29, 100786. DOI: <https://doi.org/10.1016/j.addma.2019.100786>
- [9] M. Tocci, A. Pola, L. Girelli, et al., *Metals* **2019**, 9 (3), 308. DOI: <https://doi.org/10.3390/met9030308>
- [10] ASTM International G32-16, *Standard Test Method for Cavitation Erosion Using Vibratory Apparatus*, **2016**.
- [11] ASTM International G134-17, *Test Method for Erosion of Solid Materials by Cavitating Liquid Jet*, **2017**.
- [12] A. Lichtarowicz, *J. ASTM Int.* **1979**, 664, 530–549. DOI: <https://doi.org/10.1520/STP35816S>
- [13] M. Dular, *Wear* **2016**, 346/347, 78–86. DOI: <https://doi.org/10.1016/j.wear.2015.11.007>

Research Article: Cavitation-induced wear can be found in many fluid power components. The effects of additively manufactured materials on the resistance to cavitation erosion were investigated, compared to conventional manufacturing. Mass loss and the surface structure were measured as the main indicators of cavitation erosion.

Cavitation Erosion Resistance of Additively Manufactured Materials

Fabian Guse*, Maximilian Voshage,
Johannes H. Schleifenbaum,
Katharina Schmitz

Chem. Eng. Technol. **2022**, *45* (XX),
XXX ... XXX

DOI: 10.1002/ceat.202200340

